A coupled model for reactive flow through deformable fractures in Enhanced Geothermal Systems

Salimzadeh, S.; Nick, H.M.

Published in:
Geothermics

Link to article, DOI:
10.1016/j.geothermics.2019.04.010

Publication date:
2019

Document Version
Publisher's PDF, also known as Version of record

Geothermics 81 (2019) 88–100

Contents lists available at ScienceDirect

Geothermics

journal homepage: www.elsevier.com/locate/geothermics

A coupled model for reactive flow through deformable fractures in Enhanced Geothermal Systems

S. Salimzadeh[a,b,*], H.M. Nick[a]

[a] Danish Hydrocarbon Research and Technology Centre (DHRTC), Technical University of Denmark, Lyngby, Denmark
[b] Commonwealth Scientific and Industrial Research Organisation (CSIRO), Clayton, Australia

ARTICLE INFO

Keywords:
Reactive transport
Dissolution and precipitation
Mechanical compression
Coupled
THMC model

ABSTRACT

Reactive flow through fractures results in dissolution/precipitation of minerals and thus alteration in fracture apertures/opening, affecting the flow paths in the fracture. Backed by laboratory experiments, the openings in fracture due to dissolution are most likely not stable under confining stresses, resulting in closure of fractures. In this research, a novel method to couple Thermal-Hydraulic-Mechanical (THM) with Chemical (C) processes is presented, capable of capturing the aperture closure under *in situ* stresses during heat withdrawal from an Enhanced Geothermal System (EGS). The dissolution process of silica is considered, resulting in a relatively uniform aperture increase in the fracture prior to applying the *in situ* stresses. Then, the mechanical equilibrium is solved and the final apertures are computed from the updated contact stresses on fracture surfaces. Due to the matrix compliance, in most cases the closure of the apertures induced by the uniform dissolution of silica has been observed. The results are compared against a case where the mechanical equilibrium after the dissolution process is not considered (*i.e.* one-way coupling of THM and C). Without mechanical feedback on the dissolution apertures, the flow in the fracture is dominated by dissolution apertures, also affecting the heat production from EGS. However, after applying *in situ* stresses, the effect of dissolution apertures on the heat production is diminished. Depending on the compliance of the matrix, the size of the fracture and the size of dissolution opening, the stresses are redistributed to satisfy the mechanical equilibrium, affecting the aperture distribution over the fracture.

1. Introduction

Fractures play a crucial role in energy extraction from fractured reservoirs. In geothermal reservoirs, a cold fluid is circulated through the hot, normally low-permeability rock, either by means of natural or engineered fractures. In this process, the *in situ* state variables including the stress, fluid pressure, temperature and chemical equilibrium of minerals are altered. Such coupled, multi-physics processes are encountered in other subsurface activities including CO_2 sequestration, nuclear waste disposal, acid fracturing, and secondary oil recovery. Due to the complexity of the problem and the number of parameters involved, modelling of these processes is viable primarily through numerical methods (McDermott et al., 2006). While coupling between thermal (T), hydraulic (H), and mechanical (M) processes are relatively straightforward, the feedback of chemical (C) reactions *i.e.* dissolution and precipitation of minerals, on the mechanical deformation is not well-understood. However, in a fractured reservoir, the mechanical deformation of fracture and matrix controls the fracture aperture and hydraulic conductivity.

Several coupled THM models have been proposed for fractured porous media (Ghassemi and Zhou, 2011; Guo et al., 2016; Pandey et al., 2017; Salimzadeh et al., 2016; Vik et al., 2018; Salimzadeh et al., 2018a). Fractures are the main flow paths in low-permeability rocks as normally encountered in Enhanced Geothermal Systems (EGS). The hydraulic conductivity of fractures strongly depends on the aperture. The flow through fractures is commonly expressed by the cubic law which is derived from the general Navier-Stokes equation for flow of a fluid between two parallel plates (Zimmerman and Bodvarsson, 1996). Any change in the *in situ* stresses acting on the fracture planes due to change in the fluid pressure and/or the rock matrix temperature can strongly affect the fracture apertures. Other coupled models have been proposed for fracturing media in which the fractures geometry alter due to the tensile or shear propagation of fractures (Norbeck et al., 2016; Salimzadeh et al., 2018b; Fu et al., 2011). Alteration of *in situ* pressure and temperature changes the equilibrium concentration of minerals in the fluid within fracture and that triggers dissolution/precipitation of

* Corresponding author at: Commonwealth Scientific and Industrial Research Organisation (CSIRO), Clayton, Australia.
E-mail address: saeed.salimzadeh@csiro.au (S. Salimzadeh).

https://doi.org/10.1016/j.geothermics.2019.04.010
Received 20 October 2018; Received in revised form 3 March 2019; Accepted 25 April 2019

reactive minerals. Thus, the fracture aperture (*i.e.* conductivity) can be further affected by the chemical reactions between the rock matrix and the fluid in the fracture. The effect of reactive flow on porosity/permeability of the rock through precipitation/dissolution of minerals is well understood in the literature (Babaei and Sedighi, 2018; Walsh et al., 2017).

Experimental investigations of reactive flow through fractures have confirmed increases in fracture transmissivity due to dissolution of minerals when samples were subjected to flow of under-saturated fluid with respect to the predominant minerals of the fracture surfaces (Dijk et al., 2002; Leprovost et al., 2003; Deng et al., 2016). The magnitude and distribution of chemically-induced apertures are controlled by chemical reaction rates and convective mass transport rate of dissolved minerals, quantified mainly by Damköhler number (*i.e.* reaction rate divided by the convective mass transport rate). Higher Damköhler number results in rapid saturation of the fluid with respect to the predominant mineral, creation of instabilities in the reaction front and formation of dissolution channels (Hanna and Rajaram, 1998; Detwiler et al., 2003; Szymczak and Ladd, 2006). On the other hand, in small Damköhler numbers the fluid remains under-saturated, and the dissolution becomes uniform across the fracture. For instance, in carbonate rocks with calcite as the primary mineral, the reaction rates are much higher, and creation of dissolution channels is more likely, whereas in silica-rich rocks, the solution of silica is relatively slow, and uniform dissolution is more likely. Although, the experimental studies have shown that even for silica-dominated rocks with less than 5% calcite, the calcite is responsible for porosity changes due to dissolution (André et al., 2006; Bächler and Kohl, 2005; Taron et al., 2009). It is worth mentioning that the mineral heterogeneity can also affect the formation of dissolution channels.

Fractures in deep reservoirs are under compression and a change in fracture apertures due to the chemical reaction affects the stress distribution over the contacting asperities. Dissolution of the contacting asperities can lead to the fracture closure as shown experimentally by Detwiler (2008). Although, dissolution of open regions may increase apertures locally, but dissolution of contacting asperities often reduce the overall transmissivity of the fracture (Lin and Daily, 1990; Moore et al., 1994). This aspect has not been accounted for in the current models dealing with coupled THM and C processes in the literature. Commonly, the dissolution aperture has been linearly combined with the aperture from THM processes *i.e.* the loosely or one-way coupled model (*cf.* Pandey et al., 2014, 2015; Rawal and Ghassemi, 2014). In this research, a novel two-way coupling method is presented for Thermal-Hydraulic-Mechanical-Chemical (THMC) processes, in which the remaining aperture due to mineral dissolution is computed after satisfying the mechanical equilibrium. The dissolution apertures have been introduced as gaps (openings) into the contact model, the mechanical equilibrium is satisfied, then the remaining apertures are computed from either the updated contact stresses (if two surfaces of the fracture are in contact) or the differential displacement of the two surfaces (if the fracture is in opening mode). Both approaches are implemented into a robust finite element discrete fracture-matrix (DFM) model (Salimzadeh et al., 2018a). The results for both one-way and two-way coupling are presented and compared.

2. Computational Model

2.1. Governing Equations

In the present study, fractures are modelled as discrete surfaces in the three-dimensional matrix (Paluszny and Zimmerman, 2011). The single-phase flow through fractures is defined using lubrication equation, while the matrix is assumed impermeable. Hydraulic loading, as well as the tractions due to the contact between fracture surfaces, are applied on the fracture walls. The elastic deformation model is expressed satisfying the condition of equilibrium on a representative elementary volume (REV) of the porous medium as

$$\mathrm{div}(\mathbf{D}\boldsymbol{\varepsilon} - \beta_s K(T_m - T_0)\mathbf{I}) + \mathbf{F} + (\boldsymbol{\sigma}_c - p_f \mathbf{n}_c)\delta(\mathbf{x} - \mathbf{x}_c) = 0 \tag{1}$$

where, $\mathbf{D}$ is the drained stiffness matrix, $\boldsymbol{\varepsilon} = (\nabla\mathbf{u} + \nabla\mathbf{u}^T)/2$ is the strain, $\mathbf{u}$ is the displacement vector, K is bulk modulus of rock, β_s is the volumetric thermal expansion coefficient of the rock matrix, T_m is the matrix temperature, T_0 is the initial temperature, $\mathbf{I}$ is the second-order identity tensor, $\mathbf{F}$ is the body force per unit volume, p_f is the fluid pressure in fracture, $\mathbf{n}_c$ is the outward unit normal to the fracture surface (on both sides of the fracture), $\boldsymbol{\sigma}_c$ is the contact traction on the fracture surface, $\delta(\mathbf{x} - \mathbf{x}_c)$ is Dirac delta function, and $\mathbf{x}_c$ represents the position of the fracture.

Assuming a high aspect ratio fracture that has a lateral extent much larger than its aperture, the fluid flow through deformable fracture can be written as

$$\mathrm{div}\left(\frac{{a_f}^3}{12\mu_f}\nabla p_f\right) = \frac{\partial a_f}{\partial t} + a_f c_f \frac{\partial p_f}{\partial t} - a_f \beta_f \frac{\partial T_f}{\partial t} \tag{2}$$

where, a_f is the fracture aperture, μ_f is the fluid viscosity, T_f is the fluid temperature in the fracture, and, c_f and β_f are coefficients of the fluid compressibility and volumetric thermal expansion, respectively. The governing equation for heat transfer through the fluid in the fracture can be obtained by combining Fourier's law with an energy balance for the fluid. The advective heat transfer through the fluid in the fracture can be written as

$$\mathrm{div}(a_f \boldsymbol{\lambda}_f \nabla T_f) = a_f \rho_f c_{hf} \frac{\partial T_f}{\partial t} - a_f \beta_f T_f \frac{\partial p_f}{\partial t} + a_f \rho_f c_{hf} \mathbf{v}_f . \nabla T_f - \lambda_n \frac{\partial T}{\partial n_c} d\Gamma \tag{3}$$

where, $\boldsymbol{\lambda}_f$ is the thermal conductivity tensor of the fluid, ρ_f is the fluid density, c_{hf} is the fluid heat capacity, $\mathbf{v}_f$ is the fluid velocity in fracture, and λ_n is the average thermal conductivity of the rock matrix along the direction normal to the fracture (in the direction of $\mathbf{n}_c$). The governing equation for heat conduction through the rock matrix can be obtained by combining Fourier's law with an energy balance for saturated rock as

$$\mathrm{div}(\boldsymbol{\lambda}_m \nabla T_m) = \rho_m c_{hm} \frac{\partial T_m}{\partial t} - \beta_s K T_m \frac{\partial(\mathrm{div}\,\mathbf{u})}{\partial t} + \lambda_n \frac{\partial T}{\partial \mathrm{n}_c}\delta(\mathbf{x} - \mathbf{x}_c) \tag{4}$$

where, $\boldsymbol{\lambda}_m = (1-\phi)\boldsymbol{\lambda}_s + \phi\boldsymbol{\lambda}_f$ is the average thermal conductivity tensor of the matrix, $\boldsymbol{\lambda}_s$ is the thermal conductivity tensor of the rock, $\rho_m c_{hm} = (1-\phi)\rho_s c_{hs} + \phi\rho_f c_{hf}$, ρ_s is the rock density, and c_{hs} is the rock heat capacity. More details on the governing equations for non-isothermal flow through fractures in deformable, low-permeability matrix (THM model) can be found in (Vik et al., 2018; Salimzadeh et al., 2018a, b).

The governing equation for the reactive transport through the fracture can be written as

$$\mathrm{div}[a_f D_f \nabla(\rho_f C_f)] = \frac{\partial(a_f \rho_f C_f)}{\partial t} + a_f \mathbf{v}_f . \nabla(\rho_f C_f) + R_c \tag{5}$$

where, D_f is the dispersion coefficient, ρ_f is the density of the fluid, C_f is the concentration of dissolving mineral in the fracture fluid (mol/kg), and R_c is the reaction (dissolution/precipitation) rate of the mineral (mol/m^{2}s). Dissolution or precipitation of the mineral occurs when the local concentration of the mineral deviates from the equilibrium concentration (C_{eq}). When the fluid is oversaturated with respect to the predominant mineral ($C_f > C_{eq}$), precipitation occurs. When the fluid is under-saturated ($C_f < C_{eq}$), dissolution occurs. For instance, precipitation of silica within a fracture occurs when a reduction in fluid temperature causes silica solubility to drop below the local concentration of dissolved silica (Dempsey et al., 2012). The manner in which the precipitation or dissolution reactions proceed depends on reaction rate and fluid velocity (Phillips, 1992). In this study, the reaction rate for amorphous silica/quartz is used (Pandey et al., 2015; Rawal and Ghassemi, 2014; Rimstidt and Barnes, 1980). However, any other

reaction model for any minerals can be used for the purpose of the present study. The reaction rate is defined as

$$R_c = k_+\left(1 - \frac{C_f}{C_{eq}}\right) \tag{6}$$

where, k_+ is the temperature dependent reaction rate constant (mol/m^{2}s). For amorphous silica k_+ is defined as (Rimstidt and Barnes, 1980)

$$k_+ = 10^{(-0.369-7.89\times10^{-4}T_f-\frac{3438}{T_f})} \tag{7}$$

where, T_f is the fluid temperature in Kelvin. The temperature-dependent equilibrium concentration of the amorphous silica is given by (Rimstidt and Barnes, 1980)

$$C_{eq} = 10^{(-0.338-7.889\times10^{-4}T_f-\frac{840.1}{T_f})} \tag{8}$$

2.2. Fracture Aperture Evolution under THMC Processes

Hydraulic aperture of fractures can be divided into two parts: (i) fracture aperture when two sides of the fracture are in contact. This aperture is referred to as *contact aperture* hereinafter. (ii) Fracture aperture when two sides of the fracture are not in contact and fracture is in opening mode. This aperture is referred to as *displacement aperture* hereinafter. Since the fractures are modelled as piecewise planer surfaces, in contact mode, the normal differential displacement of two sides of fracture is zero, while in the opening mode the normal differential displacement of two sides of the fracture is not zero. When two sides of a fracture are in contact, the fracture asperities are responsible for carrying compression and satisfying the mechanical equilibrium. The fracture can still be hydraulically conductive due to the roughness of the fracture surfaces. The contact aperture of the fracture is commonly defined as a function of the normal contact traction

$$a_f^c = f(\sigma_n) \tag{9}$$

where a_f^c is the contact aperture, and σ_n is the normal contact stress. Both linear and nonlinear equations can be used to express the relation between contact aperture and contact stress. In this study, the contact aperture – contact stress relationship is defined using the classical Barton-Bandis model (Bandis et al., 1983; Barton et al., 1985) as

$$a_f^c = a_0 - \frac{a\sigma_n}{1 + b\sigma_n} \tag{10}$$

in which, $a_0 = 0.0012$ m, $a = 1.6 \times 10^{-10}$ m/Pa and $b = 1.33 \times 10^{-7}$ 1/Pa. If the contact stress reduces to zero, separation of two fracture surfaces occurs, and contact aperture reaches to its maximum value of $a_f^c = a_0$. In the opening mode, the fracture asperities are not in contact anymore, thus the bulk matrix is carrying the compression, satisfying the mechanical equilibrium of the system. In subsurface activities where the fractures are initially under compression, the separation of fracture surfaces can occur due to fluid pressure exceeding the *in situ* stress, and/or thermo-poroelastic contraction of the matrix. The classical example in which the fluid pressure exceeds the *in situ* stress is the hydraulic fracturing process. When separation occurs, the displacement aperture can be defined explicitly by the normal differential displacement of two opposite surfaces of fracture as

$$a_f^d = (\mathbf{u}^+ - \mathbf{u}^-).\,\mathbf{n}_c \tag{11}$$

in which, a_f^d is the displacement aperture, $\mathbf{u}^+$ and $\mathbf{u}^-$ are the displacements of the two opposing faces of the fracture, and $\mathbf{n}_c$ is the outward unit normal to the fracture surfaces. Thus, the total aperture of a fracture is the sum of the contact and the displacement apertures

$$a_f = a_f^c + a_f^d \tag{12}$$

In cases where a fracture is freshly created such as in hydraulic fracturing, the contact aperture is zero, $a_f^c = 0$, and the displacement aperture is providing the hydraulic conductivity of the fracture. On the other hand, in natural fractures under compression, the displacement aperture is zero, $a_f^d = 0$, and the hydraulic conductivity of the fracture results from the contact aperture. Fracture aperture variation due to shear dilation can also be added to the contact aperture, however, such aperture variation is not considered in this study.

In this study, the fractures are modelled as surface discontinuities in the 3D matrix, thus the model is capable of capturing both contact and displacement apertures. When fracture surfaces are in contact, the differential displacement (Eq. 11) is zero, and the contact aperture is computed from Eq. (10). If the surfaces of fracture are not in contact, a differential displacement is computed from Eq. (11) as the displacement aperture. When fractures are modelled as surface discontinuities, under compressive loading the contact stresses (normal and shear) are required to be computed accurately, and applied on the fracture surfaces in order to avoid the inter-penetration of the fracture surfaces. The contact constraints are enforced by using a gap-based Augmented Lagrangian (AL) method (Wriggers and Zavarise, 1993; Puso and Laursen, 2004; Nejati et al., 2016). Penalties are defined at each timestep as a function of local aperture, so that they are larger away from the fracture edges, and reduce to zero at the fracture edges (fracture tips). The augmentation process makes it possible to strictly penalise any violation of contact constraints by using a small penalty parameter. More details on the contact model can be found in (Nejati et al., 2016). The contact model has been extended to include thermal and hydraulic loadings (Vik et al., 2018).

In the contact model, gaps can be implicitly introduced so that the two sides of the fracture have an initial aperture prior to loading. When the compressive load is applied, due to the initial gap at some parts of the fracture, the area of the fracture in contact is initially less than the total area of the fracture, therefore stress redistribution occurs and the parts with initial gaps deform to satisfy the mechanical equilibrium. The deformation of the matrix under compression may result in closure of the initial gap; however, the initial contact stress distribution will be affected by the existence of the initial gap. To demonstrate this property of the contact model, two examples of a fracture with an initial gap are presented in this section. A circular fracture of radius 100 m is considered within a linear elastic, homogenous, isotropic matrix with Young's modulus $E = 50$ GPa and Poisson's ratio $\nu = 0.25$. The matrix is under uniform compressive stress of 64 MPa. An initial gap is prescribed within a circular area of radius 10 m at the centre of fracture (gap area). Two distributions are considered for the initial gap: uniform and linear distributions as shown in Fig. 1. In the uniform case, an initial gap of 1 mm is assigned to the gap area in the centre of the fracture as shown in Fig. 1a. After the compressive loads are applied and solved for the equilibrium, the normal contact stress distribution is as given in Fig. 1b. Without any gap in the fracture, a uniform stress of 64 MPa is expected to develop everywhere in the model. But due to the existing gap in the fracture, stress concentration as much as 125 MPa are observed at the edges of the gap area, while the contact stress in the centre of the gap area reduces to less than the applied value (64 MPa). Also, stress relaxation is observed in a ring outside, and close to the edges of the gap area. In the second case, the initial aperture linearly increases from zero at the edges of the gap area towards 1 mm in the centre as shown in Fig. 1c. The normal contact stress in this case increases towards the centre of the fracture, while stress relaxation is observed at the vicinity of the edges of the gap area. The contact stress variation in the second case is less than the first case. The normal contact stress on the remaining parts of fracture away from the gap area in both cases is equal to the applied compression of 64 MPa.

When the fluid in fracture reacts with the rock matrix, the dissolution/precipitation of minerals also results in the aperture variation in fracture. Assuming that the rock matrix consists of one dominant reactive mineral, the variation in the aperture can be approximated from the reaction rate as (Pandey et al., 2015; Rawal and Ghassemi, 2014)

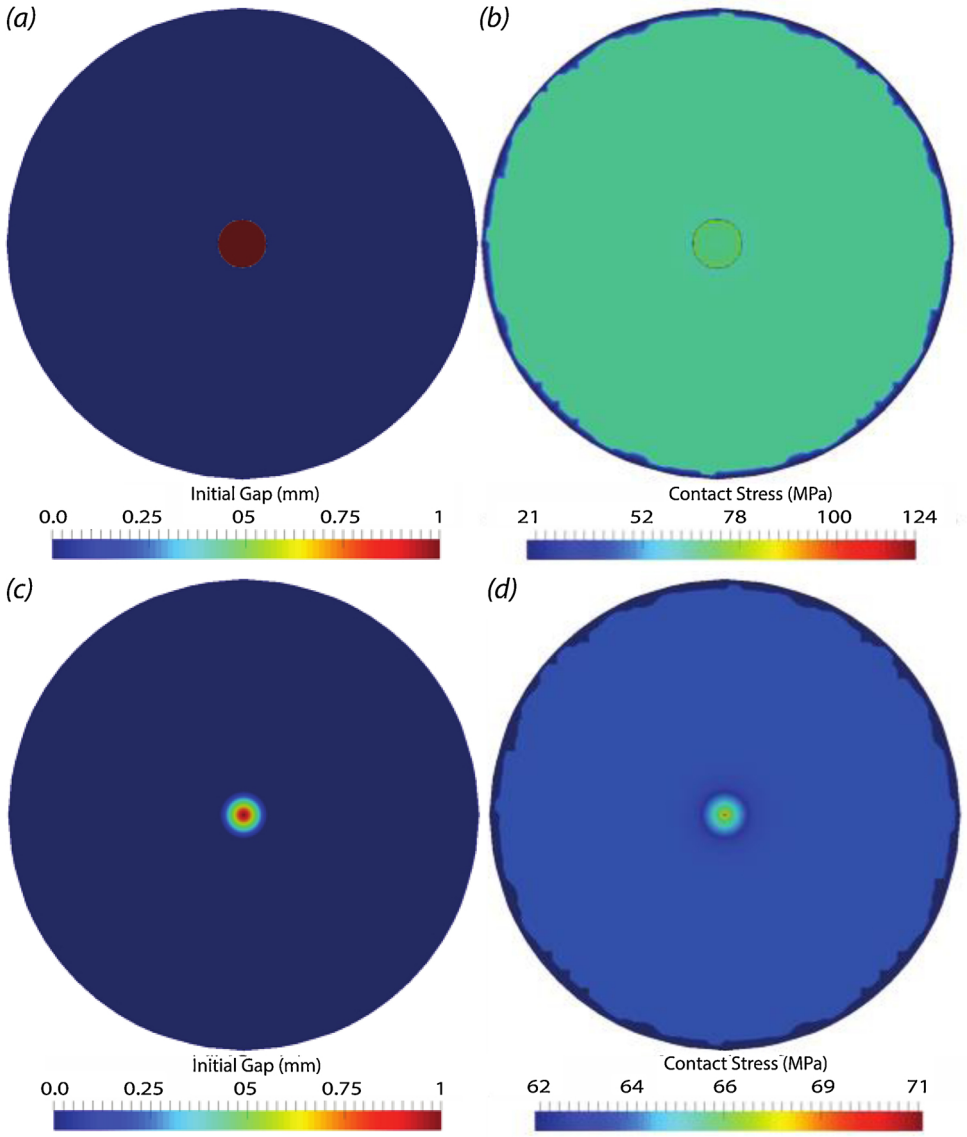

Fig. 1. Initial gap in the fracture and its effect on the contact stress distribution: (a,b) uniform initial gap, (c,d) linear initial gap distribution over an area of radius 10 m in a fracture of radius 100 m. Contact stresses at the edge of fracture are zero.

$$\frac{\partial a_c}{\partial t} = \frac{R_c}{\rho_s w} \tag{13}$$

where, $\rho_s w$ is the molar density, ρ_s is the density of the solid (rock), and w is the number of moles of the reactive mineral per kilogram of rock. The fracture aperture induced by dissolution or precipitation processes is referred to as *chemical aperture*, a_c, hereinafter. The dissolution process is of particular interest in the present study. The chemical aperture is commonly considered as an additional term to the contact aperture (Pandey et al., 2015; Rawal and Ghassemi, 2014), thus, the total aperture is written as

$$a_f = a_f^c + a_f^d + a_c \tag{14}$$

which means that chemical aperture, irrespective of its value, are considered hydraulically open and mechanically stable under *in situ* stresses. In other words, the chemical aperture is treated as "contact aperture", in which some asperities are responsible for carrying the compression between two surfaces of a fracture. Therefore, the chemical apertures directly affect the fracture conductivity, and as such, affect flow and heat transfer in the fracture. This type of coupling chemical reactions with thermo-poroelastic processes is referred to "loosely" or "one-way coupling", denoted by *THM + C*, hereinafter. In THM + C, it is assumed that the chemical apertures are not affected by the mechanical compression. However, the opening in the fracture aperture due to dissolution may not remain open under the mechanical compression as demonstrated earlier by two examples (shown in Fig. 1), and backed by the experimental investigations. To remove this deficiency, a novel approach of coupling THM and C is proposed in this study, in which, the chemically-induced apertures are treated as a "displacement aperture", subject to mechanical compression. So, in order for the chemical apertures to remain open and conductive for flow, the rock matrix has to carry the extra load due to loss of contact area where the dissolution occurs. In this approach, the chemical apertures due to dissolution are introduced as initial gaps in the fracture, then the mechanical compression is applied, and the remaining aperture (gap) is determined after satisfying the mechanical equilibrium. If the chemically-induced gap remains open in some areas, then the contact stress in those areas will be zero and the displacement aperture is computed from Eq. 11. If the dissolution gap is closed due to the compliance of the rock matrix under compression, the contact stresses are updated, and the new contact apertures are computed from Eq. 10. Thus, depending on the compression that the fracture receives

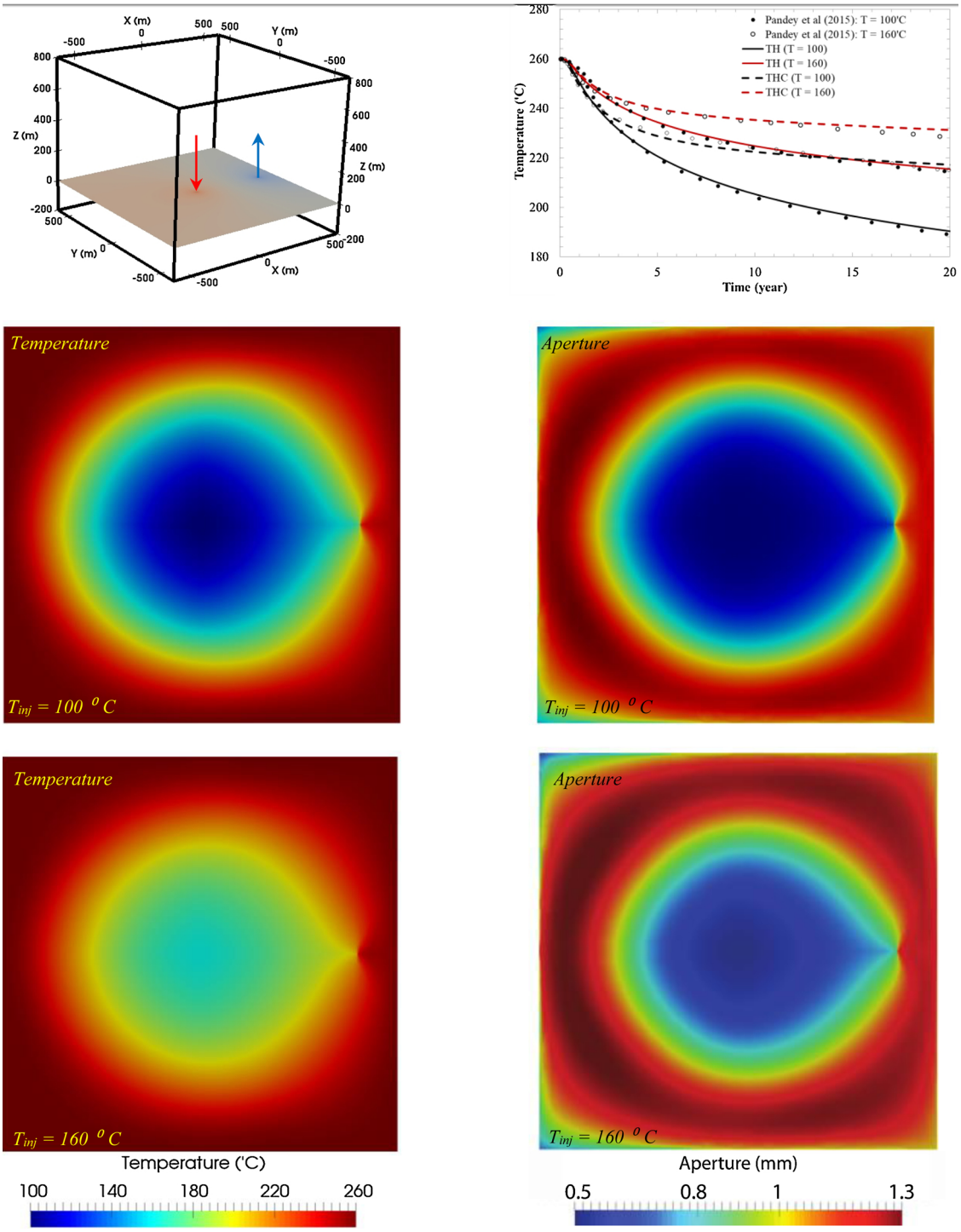

Fig. 2. The geometry and simulation results for the validation example.

and compliance of the rock matrix, part of or perhaps the whole new gap from the chemical dissolution may be closed. For convenience, this approach of coupling THM and C is referred to as *THMC* hereinafter. In THMC, the coupling between THM and C is two-way as the chemical apertures are affected by the mechanical compression, and at the same time, the stresses are affected by the chemical apertures.

2.3. Finite Element Model

The governing equations are solved numerically using the finite element method. Spatial and temporal discretisation are realised using Galerkin method and finite difference techniques, respectively. The displacement vector $\mathbf{u}$, the fluid pressure in fracture p_f, fluid temperature T_f, rock matrix temperature T_m, and mineral concentration in fracture C_f are taken as primary variables. Using the standard Galerkin method, the primary variable $\mathbb{X} = \{\mathbf{u}, p_m, p_f, T_m, T_f, C_f\}$ within an element is approximated from its nodal values as

$$\mathbb{X} = \mathbf{N}\hat{\mathbb{X}} \tag{15}$$

where $\mathbf{N}$ is the vector of shape functions and $\hat{\mathbb{X}}$ is the vector of nodal values. Using the finite difference technique, the time derivative of $\mathbb{X}$ is defined as

Table 1
Input properties used in the validation example.

Property	Value	Unit
Initial fracture aperture	0.5	mm
Fluid heat capacity (C_f)	4180	J/kg °C
Fluid thermal conductivity (λ_f)	0.6	W/m °C
Rock density (ρ_s)	2500	kg/m^3
Rock heat capacity (C_s)	1000	J/kg °C
Mass flow rate	40	kg/s
Injection temperature	100, 160	°C
Injection concentration	0	mol/kg
Rock thermal conductivity (λ_s)	2.5	W/m °C
Dispersion coefficient (D_f)	1×10^{-9}	m^2/s

$$\frac{\partial \mathbb{X}}{\partial t} = \frac{\mathbb{X}^{t+dt} - \mathbb{X}^{t}}{dt} \tag{16}$$

where $\mathbb{X}^{t+dt}$ and $\mathbb{X}^{t}$ are the values of $\mathbb{X}$ at time $t + dt$ and t, respectively. The set of discretised equations can be written in matrix form as $\mathbb{S}\mathbb{X} = \mathbb{F}$, in which $\mathbb{S}$ is the element's general stiffness matrix, and $\mathbb{F}$ is the vector of right-hand-side loadings. Following the approach explained in (Vik et al., 2018), the mechanical deformation-contact (M) and the thermal-hydraulic-chemical models (THC) are solved sequentially. However, the implemented model is also capable of solving the two models simultaneously. The components of the stiffness matrix are dependent upon the primary unknown variables, *i.e.* conductance, capacitance and coupling coefficients of the fracture are all dependent on the fracture aperture; therefore, a Picard iteration procedure is adopted to reach the correct solution within acceptable tolerance. For current iteration $s + 1$ in current step $n + 1$, the solution-dependent coefficient matrices in the stiffness matrix $\mathbb{S}$ are updated using weighted average solution vector $\mathbb{X}_{n+1}^{s+\theta}$ defined as

$$\mathbb{X}_{n+1}^{s+\theta} = (1 - \theta)\mathbb{X}_{n+1}^{s-1} + \theta\mathbb{X}_{n+1}^{s} \tag{17}$$

where $\mathbb{X}_{n+1}^{s-1}$ and $\mathbb{X}_{n+1}^{s}$ are the solution vectors of the two most recent iterations in the current timestep $n + 1$, and $\theta = 2/3$ is the weighting coefficient. For the first iteration $s = 1$, the previous timestep solution is used as

$$\mathbb{X}_{n+1}^{0} = \mathbb{X}_{n+1}^{1} = \mathbb{X}_{n} \tag{18}$$

where $\mathbb{X}_n$ is the solution vector from previous timestep n. The iterations are repeated until consecutive normalised values of $\mathbb{X}_{n+1}^{s}$ agree to within a specified tolerance ε

$$\frac{\|\mathbb{X}_{n+1}^{s+1} - \mathbb{X}_{n+1}^{s}\|}{\|\mathbb{X}_{n+1}^{s+1}\|} < \varepsilon \tag{19}$$

The tolerance is set to 1%. The discretised equations are implemented in the Complex Systems Modelling Platform (CSMP, also known as CSP), an object-oriented application programme interface (API), for the simulation of complex geological processes and their interactions (formerly CSP, *cf.* Matthäi et al., 2007). Quadratic unstructured elements are used for spatial discretisation of surfaces (quadratic triangles) and volumes (quadratic tetrahedra). The triangles on two opposite faces of a fracture are matched with each other, but do not share nodes, and duplicate nodes are defined for two sides of a fracture. The triangles are faces of the tetrahedra connected to the fractures, and they share nodes. Fracture flow, heat and mass transfers equations are accumulated over triangular elements (on one side of the fracture *i.e.* master side), whereas, matrix deformation and heat transfer equations are accumulated over the volume elements. The ensuing set of linear algebraic equations is solved using the algebraic multigrid method, SAMG (Stüben, 2001).

2.4. Model Verification

The THM part of the present model has been validated extensively against several analytical, experimental and numerical results published in the literature. More details can be found in (Vik et al., 2018; Usui et al., 2017; Salimzadeh et al., 2019; Peters et al., 2018). In this study, the THC part of the model is validated against the results given by Pandey et al., 2015 for the dissolution of amorphous silica in a silica-rich geothermal reservoir.

In this example, a geothermal doublet including an injection well and a production well is connected to a horizontal rectangular fracture of size 1250 × 1250 m. The reservoir layer has a thickness of 1000 m with a temperature gradient of 200 °C/km, with temperature at top of the reservoir is set to 100 °C, and at the bottom to 300 °C. The fracture is located at depth of 800 m in the layer (Fig. 2) corresponding to an initial temperature of 260 °C. The injection well intersects the centre of the fracture, and the production well is located 500 m away from the injection well. The properties of the problem are given in Table 1. The matrix is considered permeable in the original example with a permeability of 10^{-18} m^2, but since this permeability is very low compared to that of the fracture, it is ignored in this study. Two different cases are considered in which the injection temperature is set to 100 and 160 °C, and the concentration of amorphous silica at the injected water is set to zero, *i.e.* clean water. For each case both TH and THC results in terms of the production temperature is recorded and compared with the results published by Pandey et al. (2015). As there is no mechanics included in this example, the chemical apertures are simply added to that of TH (*i.e.* uniform initial aperture). As shown in Fig. 2, a good match is observed between two simulations, for both TH and THC processes, confirming the accuracy of the THC module of the present model. Included in Fig. 2, are the temperature and aperture distribution after 20 years for both cases. The injection of clean water results in dissolution of amorphous silica, while the *in situ* concentration of amorphous silica is 0.022 mol/kg of water. The reaction rate is higher where the temperature is higher, away from the injection well. Thus, the aperture increases up to 1.3 mm due to dissolution of minerals along a strip located away from the injection well. The dissolution process creates a channel for flow towards the bigger area of the fracture and away from the production well, delaying the temperature drop at the production by providing longer paths for the cold fluid to flow before reaching the production well.

3. Simulation Results and Discussion

3.1. Simulation Cases

A conceptual EGS consisting of a geothermal doublet intersecting a horizontal circular fracture in a homogenous isotropic elastic rock, as shown in Fig. 3, is considered for simulations. The geometry of the model roughly resembles the Habanero project in the Cooper Basin, Australia (Llanos et al., 2015). The material properties, adopted from Guo et al. (2016), are given in Table 2. The chemical reactions are considered for the dissolution of a mineral (amorphous silica) based on the properties used in the validation example (Pandey et al., 2015). Four different cases are considered for simulations as summarized in Table 3.

- In case I, a horizontal circular fracture of radius 500 m is considered with injection and production wells intersecting the fracture symmetrically at 500 m spacing. The far-field stress is set to 64 MPa, while the initial pressure and temperature are set to 34 MPa and 200 °C, respectively. Water is injected at a flow rate of $Q = 0.0125$ m^3/s, at a temperature of 50 °C, while the production is configured through constant pressure of 34 MPa. In this case, it is assumed that the rock has 15 mol of silica per kg, $w = 15$ mol/kg.
- In case II, the chemical apertures are magnified artificially by

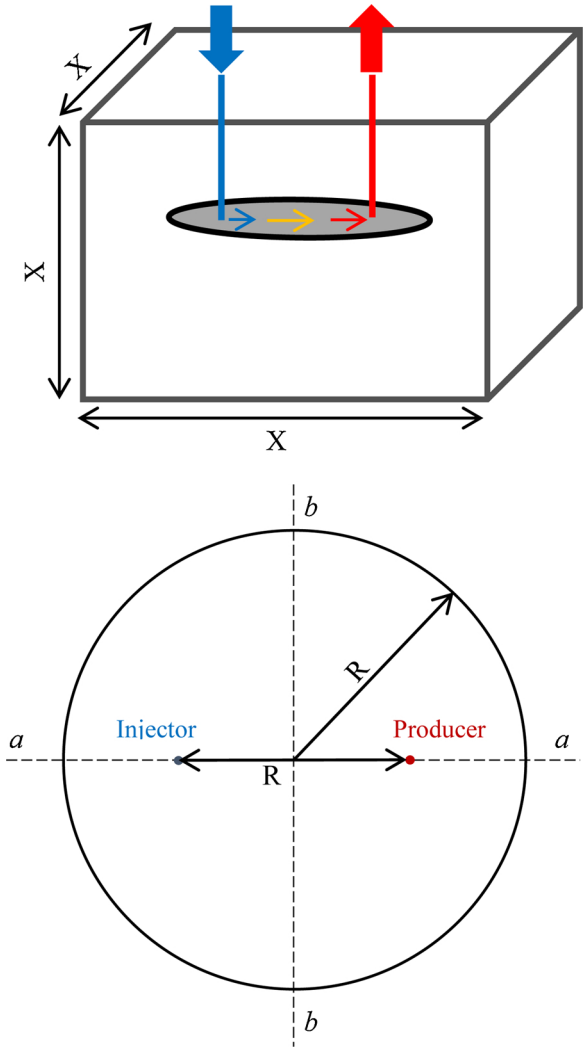

Fig. 3. The geometry of the model and the fracture used in the simulations. Three cases are: (i) X = 3 km, R = 500 m, (ii) X = 1.5 km, R = 250 m, (iii) X = 600 m, R = 100 m.

Table 2
Input properties used in the simulations.

Parameter	Value	Unit
Matrix porosity (φ)	0.01	–
Solid density (ρ_s)	2500	kg/m^3
Young's modulus (E)	50	GPa
Poisson's ratio (ν)	0.25	–
Solid heat capacity (c_{hs})	790	J/kg°C
Fluid heat capacity (c_{hf})	4460	J/kg°C
Volumetric thermal expansion coefficient of the solid (β_s)	2.4×10^{-5}	/°C
Volumetric thermal expansion coefficient of the fluid (β_f)	7.66×10^{-4}	/°C
Fluid dynamic viscosity (μ_f)	1.42×10^{-4}	Pa s
Fluid compressibility (c_f)	5.11×10^{-10}	Pa^{-1}
Thermal conductivity of the solid (λ_s)	3.5	W/m°C
Thermal conductivity of the fluid (λ_f)	0.6	W/m°C
Dispersion coefficient (D_f)	1×10^{-9}	m^2/s

reducing the molar density of silica. An alternative approach to increase the chemical apertures would be to increase either the simulation time beyond 30 years, or the dissolution rate. The former would result in excessive temperature drop at production, while the latter would change the reaction type from a relatively uniform dissolution to wormhole dissolution. Thus, the mole per kilogram of the rock has been reduced to $w = 1$ mol/kg in order to increase the chemically-induced aperture. All other parameters and boundary conditions are kept the same as case I.

- In case III, the size of the fracture is reduced to 250 m. The size of the model is also reduced accordingly, as shown in Fig. 3. The size of the fracture has been varied to investigate whether the chemical apertures remain open under *in situ* stresses in smaller fractures. To avoid the early breakthrough and rapid reduction in temperature at the production, the injection temperature has been increased to 100 °C, and the injection flow rate is reduced to 0.003125 m^3/s. All other parameters and boundary conditions are kept the same as case II.
- In case IV, the fracture (and model) size is further reduced. A 100 m fracture is considered, with a flow rate of Q = 0.001 m^3/s. All other parameters and boundary conditions are kept the same as case III.

3.2. Results and Discussion

The four cases mentioned above are simulated for five sets of different coupled physics:

1 Thermal-hydraulic (TH): In this model, only fluid flow and heat transfer are modelled within the EGS. Considering the initial contact stress is 30 MPa, the contact aperture in this set, using Eq. (10) is 0.24 mm.
2 Thermal-hydraulic-chemical (THC): In this model, fluid flow, heat transfer and chemical reactions (dissolution, precipitation) are modelled within the EGS. The chemically induced apertures are simply added to the initial aperture of 0.24 mm.
3 Thermal-hydraulic-mechanical (THM): In this model, fluid flow, heat transfer and mechanical deformation are modelled within the EGS. The apertures are computed using Eq. (10) from the updated contact stresses. Again, the initial aperture at onset of simulation is 0.24 mm.
4 Thermal-hydraulic-chemical-mechanical (THM + C): In this model, fluid flow, heat transfer, chemical reaction and mechanical deformation are modelled within the EGS. The chemically induced apertures are simply added to the contact aperture computed from updated contact stresses using Eq. 14.
5 Thermal-hydraulic-chemical-mechanical (THMC): In this model, fluid flow, heat transfer, chemical reaction and mechanical deformation are modelled within the EGS. However, the chemically induced apertures are introduced as gaps into the contact stress solver, and the final apertures are computed from the updated contact stresses using Eq. 12.

The aperture distributions over the fracture for different cases in different models: THC, THM, THM + C and THMC are shown in Fig. 4. In the THC model, the aperture variation is purely from the chemical reactions. Maximum aperture increase occurs in areas with higher temperature, thus it enhances the flow towards the remote areas of the fracture. In the THM model, the aperture variation is caused by the mechanical deformation of the matrix under THM loading. Therefore, the maximum aperture increase occurs in colder areas with higher fluid pressure, *i.e.* in the vicinity of the injection well. In the THM + C model, the distribution of aperture is a combination of that in THM and THC models. However, the aperture distribution in THMC model is very similar to the THM model, implying that the chemically-induced gaps in the fracture are closed under THM compression, even though the magnitude of dissolution apertures (*i.e.* gaps) has been magnified in cases II, III and IV. In case IV, the size of the fracture reduces, thus, the THMC model shows slightly higher apertures than the THM model due to the redistribution of stresses in the matrix.

The temperature distributions after 30 years of simulation for the four cases using the results of five different models: TH, THC, THM,

Table 3
Different cases used in simulations.

Simulation Case	Model Size (km)	Fracture Size (m)	Injection Rate ($m^3/2$)	Injection Temperature (°C)	w (mol/kg)
I	3 × 3×3	500	0.0125	50	15
II	3 × 3×3	500	0.0125	50	1
III	1.5 × 1.5 × 1.5	250	0.003125	100	1
IV	0.6 × 0.6 × 0.6	100	0.001	100	1

THM + C, and THMC, are shown in Fig. 5. As the size of the fracture reduces, larger portion of the fracture is affected by the cold fluid. When the chemical reactions are accounted for, the chemically induced apertures dominate the flow and heat transfer in both THC and THM + C models. Thus, the temperature plume extends further away from the injection and production wells, and the access to the hot matrix increases in these two models compared to the reference TH model. For instance in case IV, the chemically-induced apertures provide access for the cold fluid to almost all surface of the fracture except a small part behind the production well. However, when the mechanical deformation of the matrix and resulting contact stresses are responsible for any changes in the fracture aperture (*i.e.* in THM and

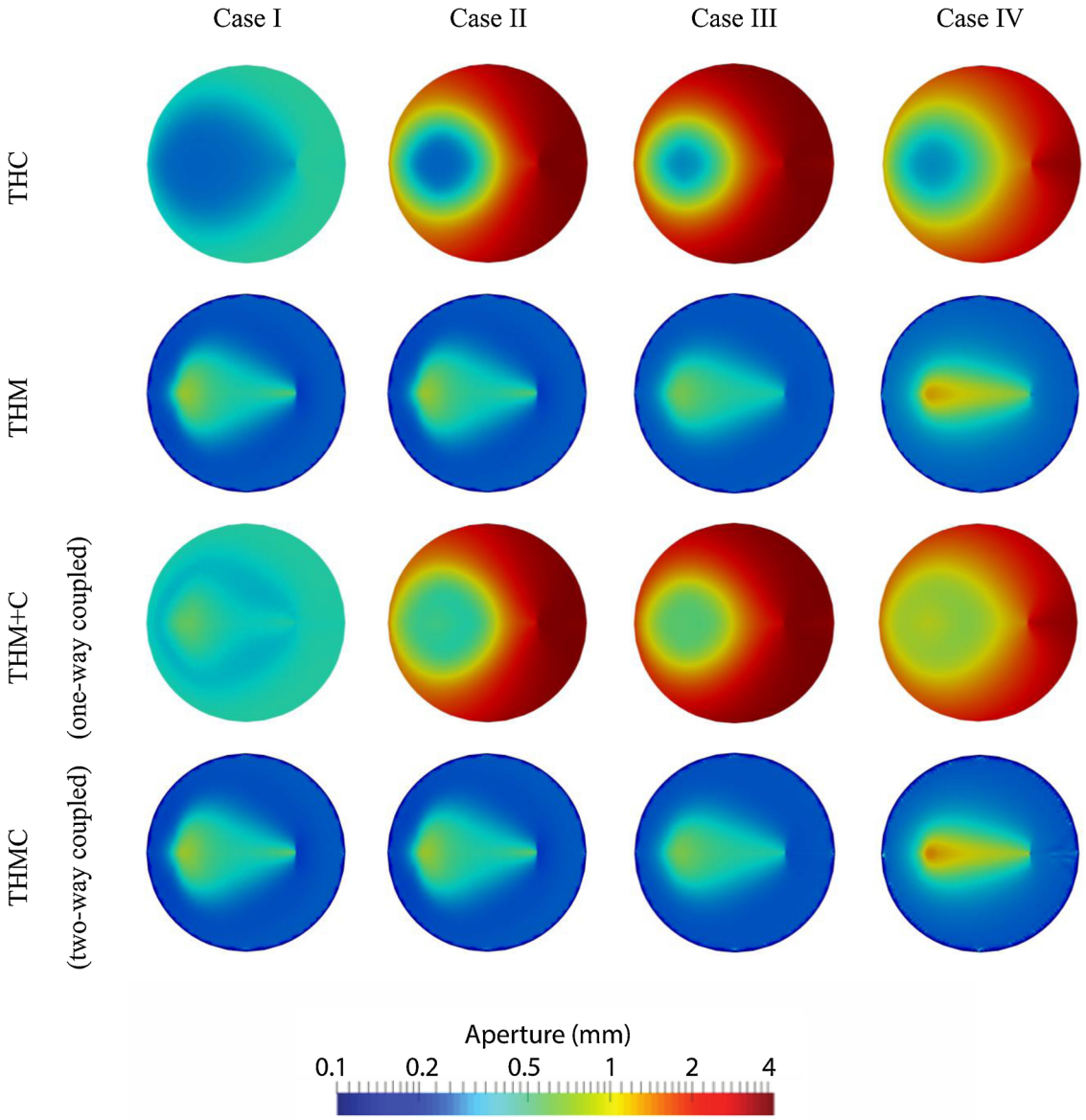

Fig. 4. Aperture distribution in fracture after 30 years for different cases presented in Table 3. THC: thermo-hydro-chemical processes, THM: thermo-hydro-mechanical processes, THM + C: thermo-hydro-mechanical- chemical processes with chemical aperture treated as contact aperture (one-way coupled), THMC: thermo-hydro-mechanical- chemical processes with chemical aperture treated as displacement aperture(two-way coupled).

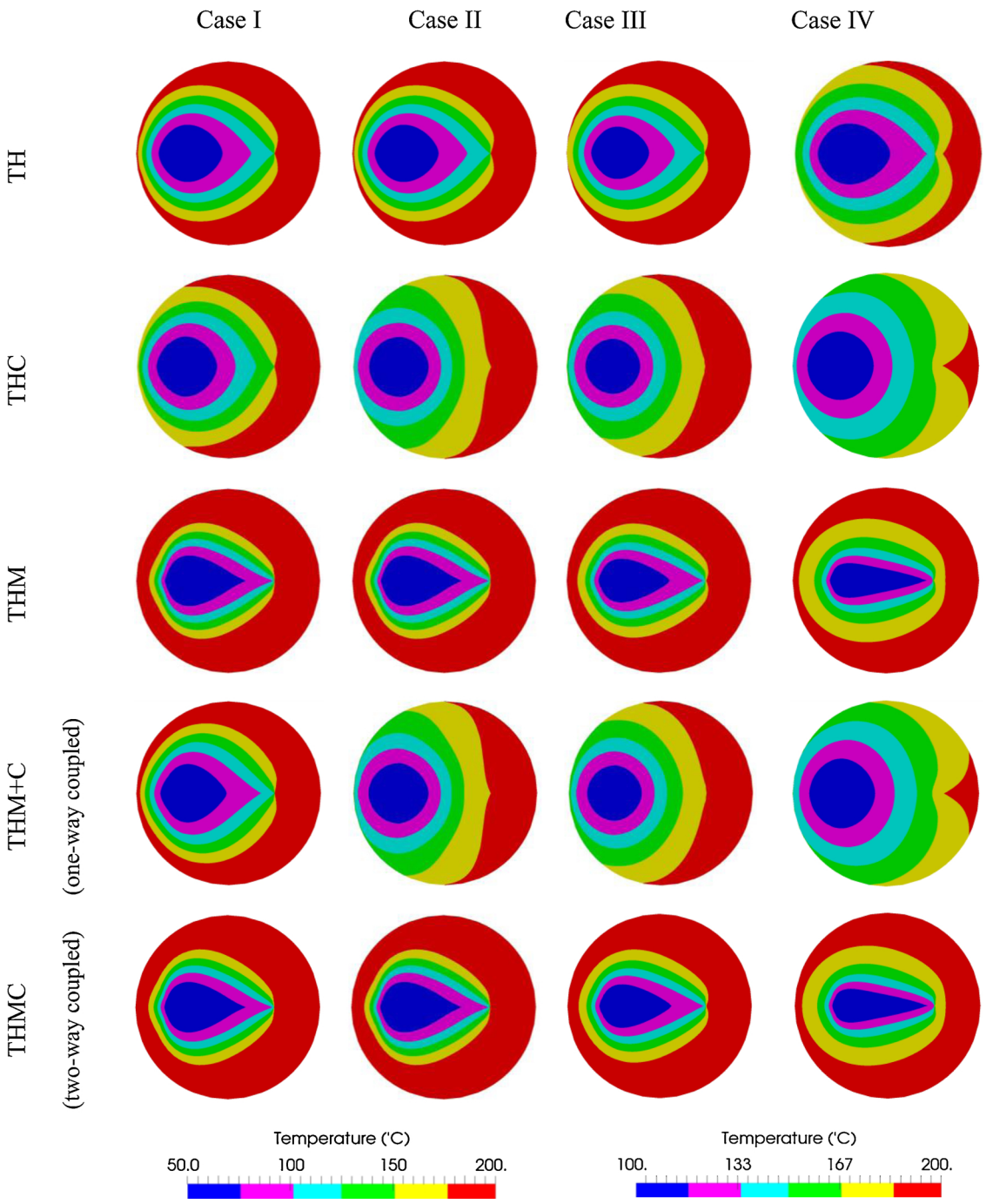

Fig. 5. Temperature distribution in fracture after 30 years for different cases presented in Table 3. THC: thermo-hydro-chemical processes, THM: thermo-hydro-mechanical processes, THM + C: thermo-hydro-mechanical- chemical processes with chemical aperture treated as contact aperture, THMC: thermo-hydro-mechanical- chemical processes with chemical aperture treated as displacement aperture.

THMC models), the cold plume stretches more towards the production well compared to the TH model. In the THMC model, the chemical reaction has no significant effect on the temperature distribution as the chemically-induced apertures are closed under the compression. The temperature distribution in the THMC model is also very similar to that of THM model. In case IV, slight differences in the temperature distribution from the THM and THMC models can be observed.

In Fig. 6, the vertical stress distributions at the end of simulation over a horizontal cut plane passing through the fracture for the three cases: II, III and IV are compared for the THM and THMC models. In the THM model, matrix contraction due to the cooling of the matrix results in a reduction of contact stress around the injection point and towards the production point. Therefore, the stresses are redistributed and an area with stress higher than the initial value (30 MPa) is developed, shown by blue colour in Fig. 6. In case II with largest fracture, that area crosses the fracture itself, while in case IV with smallest fracture, it passes through the matrix. When chemical reactions are considered and the chemical aperture is introduced as gaps in the contact model, the

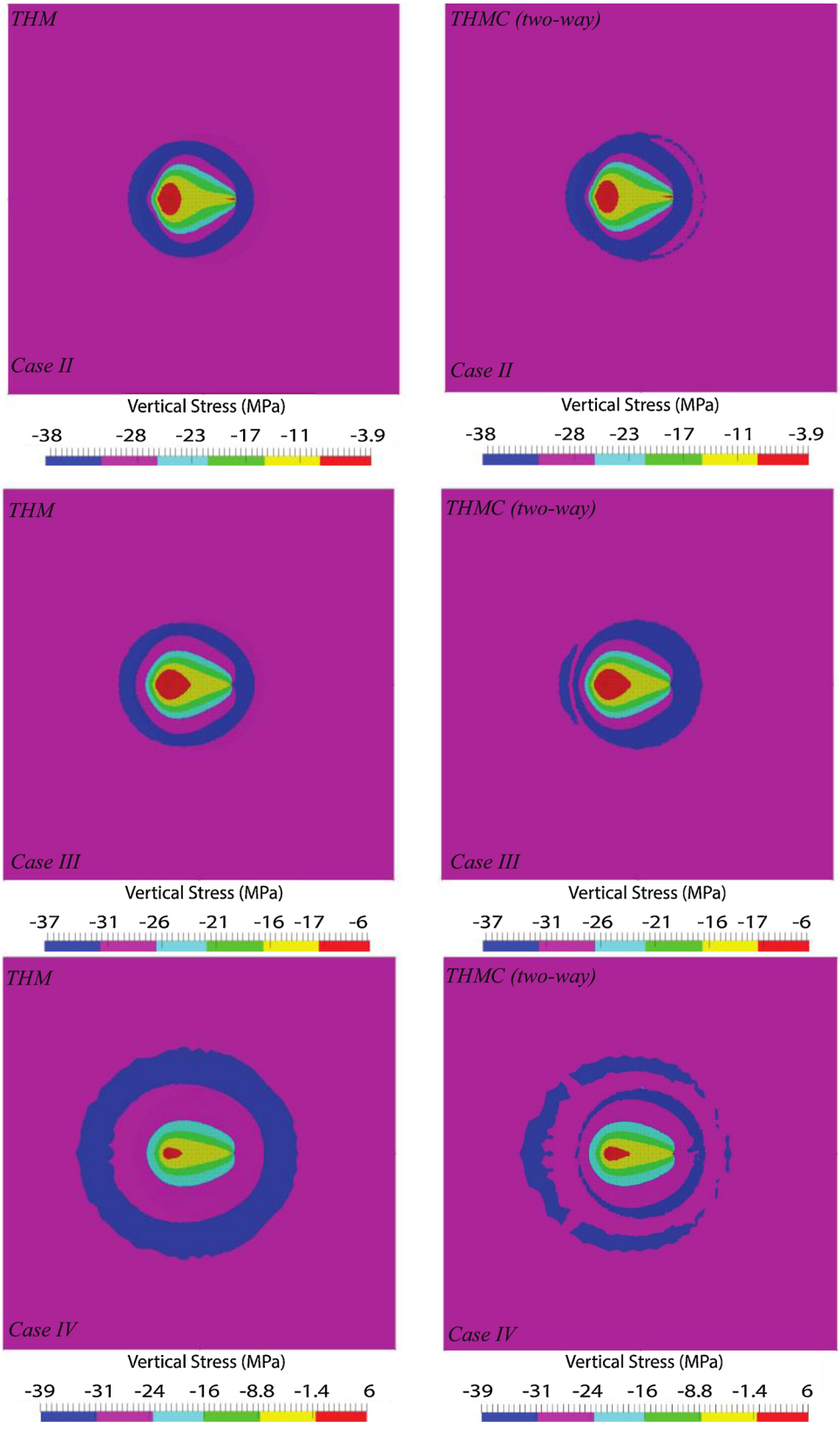

Fig. 6. Vertical stress distribution over a horizontal plane passing through the fracture.

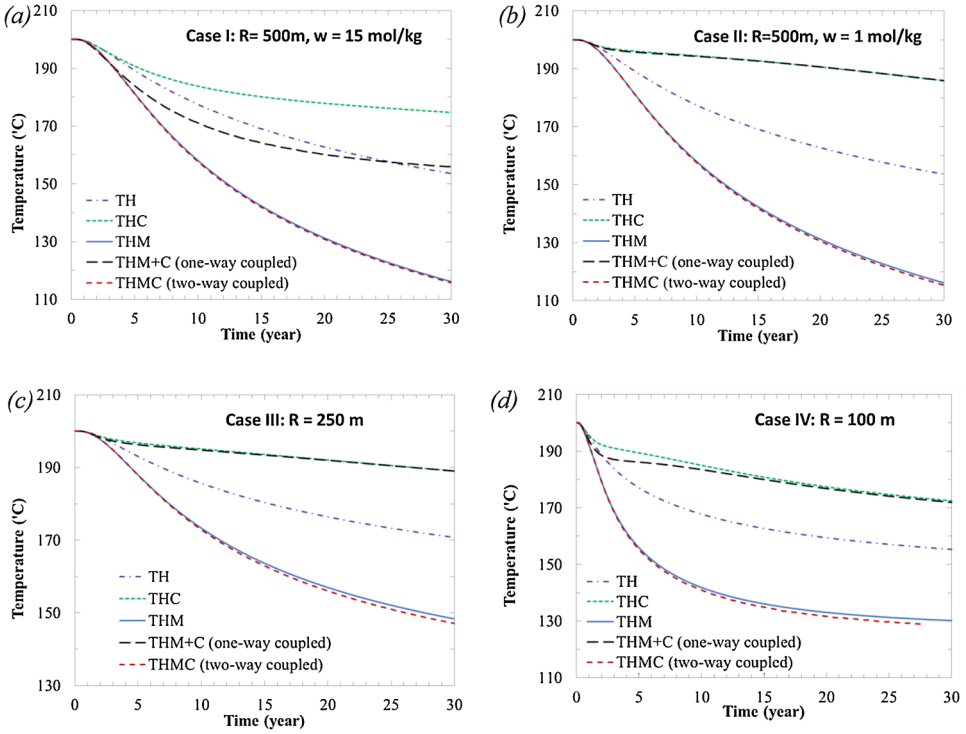

Fig. 7. Temperature drawdown at production for different cases presented in Table 3, simulated using different models.

over-stressed area expands and includes the edges of fracture. In cases II and III, the redistribution of vertical stresses has no significant impact on the lower contact stresses (shown by red colour), however, in case IV, the area of lowest contact stress in the THMC model is larger than the THM model. The lower contact stress in the THMC model results in higher aperture and thus, faster drawdown of the temperature at production. It is worth mentioning that the vertical stress around the injection well in case IV has entered the tensile region, meaning the fracture has entered the opening mode.

The evolution of temperature at production versus time for different cases is shown in Fig. 7. Results show that the chemical dissolution (C) and mechanical deformation (M) have opposite effects on the flow pattern in the fracture. The chemical dissolution creates longer paths through the remote areas of fracture for the cold fluid to travel towards the production, hence it increases the residence time of the fluid and improves the efficiency of the geothermal system. The mechanical effects, on the other hand, enhance flow channelling directly towards the production well and thus, reduces the efficiency. Referring to the results of TH model as the reference for comparison, the THC model predicts much higher heat production compared to the TH model, while the THM model shows much lower heat production from the EGS. When the effects of chemical dissolution and mechanical deformation are combined linearly as in THM + C model, the outcomes are relatively close to the TH model for case I. However, in cases II, III and IV, where the contribution of chemical dissolution is exaggerated, the outcomes of THM + C model is very similar to the THC model (*i.e.* chemical dissolution effects are dominant). The THMC model, on the other hand, predicts results very similar to the THM model. Reducing the size of fracture in case IV reduces the compliance of the matrix, thus, the chemical dissolutions in THMC model in this case deviates the THMC model results from the THM model. Unlike THC and THM + C models, THMC model shows that in case IV, the redistribution of stresses due to closure of chemically-induced gaps actually facilitates the flow channelling, decreasing the heat production from the EGS.

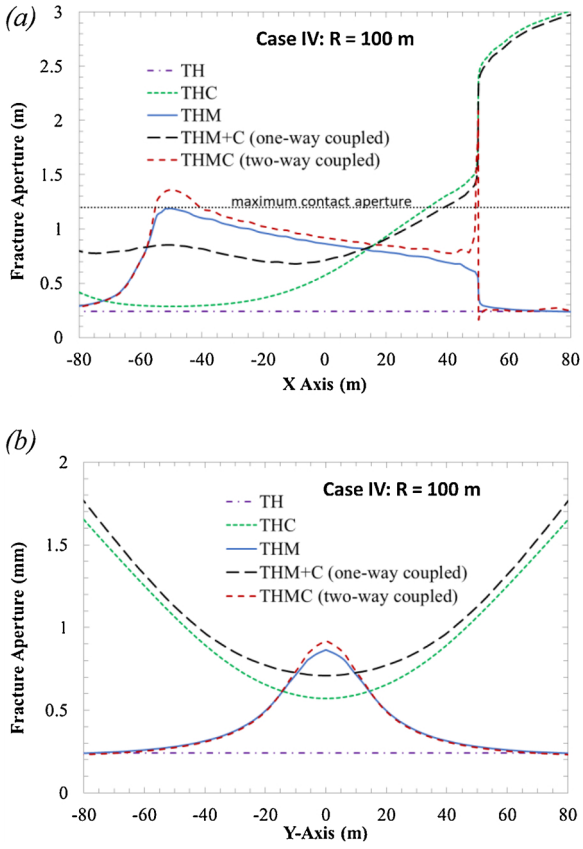

Fig. 8. Aperture distribution along two prependicular lines passing through the centre of fracture in case IV for dfferent models: (a) along *a-a* line, (b) along *b-b* lines shown in Fig. 3.

The aperture profiles along two perpendicular lines passing through the centre of fracture (*a-a* and *b-b* lines shown in Fig. 3) for case IV are shown in Fig. 8. The TH model has a constant, uniform aperture of 0.24 mm (equal to the initial aperture), while the THC model predicts higher apertures in remote regions away from the injection/production wells (towards the edges of the fracture on *a-a* line, and behind the production point on *b-b* line). This is due to higher dissolution rate at regions with higher temperature. The THM model shows higher apertures in cold areas (around the injection well and towards the production well). The THM + C model enjoys the aperture increases by both mechanical deformation (M) and chemical dissolution (C). The THMC model shows slightly higher apertures than the THM model between the injection and production points due to the stress redistribution from the gap in the fracture from the chemical dissolution, responsible for slightly lower heat production from the EGS.

4. Conclusions

Two methods for coupling thermal-hydraulic-mechanical (THM) processes with the chemical (C) reactions – mainly dissolution of minerals – are presented: one-way or loosely coupling (referred to as THM + C), and two-way coupling (referred to as THMC). The effects of two methods on heat production from an EGS are compared to each other as well as to several reduced models: thermal-hydraulic (TH), thermal-hydraulic-chemical (THC), and thermal-hydraulic-mechanical (THM). The key findings of this study are as follows:

- For dissolution of silica, the effects of chemical dissolution (C) and mechanical deformation (M) are opposite.
- Chemical dissolution improves heat production from the EGS (compared to the reference TH model) by providing access to the remote areas of the fracture where the dissolution occurs.
- Mechanical deformation reduces the heat production from the EGS (compared to the reference TH model) by facilitating the fluid flow towards the production point.
- When the effects of chemical dissolution and mechanical deformation are combined linearly (as in THM + C model), the outcomes for heat production are somewhere between the two THM and THC models. Depending on which process (M or C) is dominant, the outcomes of THM + C may get closer to either THM or THC model results.
- When the opening in fracture due to dissolution of silica is introduced as gaps and the contact stresses are resolved using the mechanical equilibrium, those dissolution gaps are mainly closed under compression in the THMC model. Thus, the outcomes are very close to the THM model.
- The closure of dissolution apertures occurs due to the compliance of the matrix. Reducing the size of the fracture in case IV increases the effects of the dissolution gaps on the contact stresses.
- The stress redistribution from closure of dissolution gaps in THMC model enhances the fluid flow towards the production point, further reducing the heat production from the EGS.
- The outcomes of the two-way coupling (THMC model) for a more reactive mineral such as calcite may be different, but it is expected that the size of the dissolution opening decreases under mechanical compression. Such deformation in the fracture results in redistribution of contact stresses, affecting the conductivity of the fracture.

Acknowledgments

Authors thank the European Union for partially funding this work through the EU Horizon 2020 research and innovation programme, under grant agreement No 654662.

References

André, L., Rabemanana, V., Vuataz, F.-D., 2006. Influence of water–rock interactions on fracture permeability of the deep reservoir at Soultz-sous-Forêts, France. Geothermics 35 (5–6), 507–531.
Babaei, M., Sedighi, M., 2018. Impact of phase saturation on wormhole formation in rock matrix acidizing. Chem. Eng. Sci. 177, 39–52.
Bächler, D., Kohl, T., 2005. Coupled thermal-hydraulic-chemical modelling of enhanced geothermal systems. Geophys. J. Int. 161 (2), 533–548.
Bandis, S.C., Lumsden, A.C., Barton, N.R., 1983. Fundamentals of rock joint deformation. Int. J. Rock Mech. Min. Sci. Geomech. Abstr. 20 (6), 249–268.
Barton, N., Bandis, S., Bakhtar, K., 1985. Strength, deformation and conductivity coupling of rock joints. Int. J. Rock Mech. Min. Sci. Geomech. Abstr. 22 (3), 121–140.
Dempsey, D.E., Rowland, J.V., Zyvoloski, G.A., Archer, R.A., 2012. Modeling the effects of silica deposition and fault rupture on natural geothermal systems. J. Geophys. Res. Solid Earth 117, B05207.
Deng, H., et al., 2016. A 2.5D Reactive Transport Model for Fracture Alteration Sreactive transport model for fracture alteration simulation. Environ. Sci. Technol. 50, 7564–7571.
Detwiler, R.L., 2008. Experimental observations of deformation caused by mineral dissolution in variable-aperture fractures. J. Geophys. Res. Solid Earth 113, B08202.
Detwiler, R.L., Glass, R.J., Bourcier, W.L., 2003. Experimental observations of fracture dissolution: the role of Peclet number on evolving aperture variability. Geophys. Res. Lett. 30 (12), 27–30.
Dijk, P.E., Berkowitz, B., Yechieli, Y., 2002. Measurement and analysis of dissolution patterns in rock fractures. Water Resour. Res. 38 (2) 5-1-5–12.
Fu, P., Johnson, S.M., Hao, Y., Carrigan, C.R., 2011. Fully coupled geomechanics and discrete flow network modeling of hydraulic fracturing for geothermal applications. In: Proceedings, Thirty-Sixth Workshop on Geothermal Reservoir Engineering, Stanford University. Stanford, California, January 31 – February 2.
Ghassemi, A., Zhou, X., 2011. A three-dimensional thermo-poroelastic model for fracture response to injection/extraction in enhanced geothermal systems. Geothermics.
Guo, B., Fu, P., Hao, Y., Peters, C.A., Carrigan, C.R., 2016. Thermal drawdown-induced flow channeling in a single fracture in EGS. Geothermics 61, 46–62.
Hanna, R.B., Rajaram, H., 1998. Influence of aperture variability on dissolutional growth Vh. Water Resour. 34 (11), 2843–2853.
Leprovost, R., Noiriel, C., Gouze, P., Bruderer, C., Loggia, D., 2003. X-ray tomography characterization of fracture surfaces during dissolution. Geophys. Res. Lett. 30 (no. 5).
Lin, W., Daily, W., 1990. Hydrological properties of Topopah Spring tuff under a thermal gradient—laboratory results. Int. J. Rock Mech. Min. Sci. Geomech. Abstr. 27 (5), 373–386.
Llanos, E.M., Zarrouk, S.J., Hogarth, R.A., 2015. Numerical model of the Habanero geothermal reservoir, Australia. Geothermics 53, 308–319.
Matthäi, S.K., et al., 2007. Numerical Simulation of Multi-phase Fluid Flow in Structurally Complex Reservoirs. Geol. Soc. London, Spec. Publ.
McDermott, C.I., Randriamanjatosoa, A.R.L., Tenzer, H., Kolditz, O., 2006. Simulation of heat extraction from crystalline rocks: the influence of coupled processes on differential reservoir cooling. Geothermics 35, 321–344.
Moore, D.E., Lockner, D.A., Byerlee, J.D., 1994. Reduction of permeability in granite at elevated temperatures. Science (80-.). 265 (5178), 1558–1561.
Nejati, M., Paluszny, A., Zimmerman, R.W., 2016. A finite element framework for modeling internal frictional contact in three-dimensional fractured media using unstructured tetrahedral meshes. Comput. Methods Appl. Mech. Eng. 306, 123–150.
Norbeck, J.H., McClure, M.W., Lo, J.W., Horne, R.N., 2016. An embedded fracture modeling framework for simulation of hydraulic fracturing and shear stimulation. Comput. Geosci. 20, 1–18.
Paluszny, A., Zimmerman, R.W., 2011. Numerical simulation of multiple 3D fracture propagation using arbitrary meshes. Comput. Methods Appl. Mech. Eng.
Pandey, S.N., Chaudhuri, A., Kelkar, S., Sandeep, V.R., Rajaram, H., 2014. Investigation of permeability alteration of fractured limestone reservoir due to geothermal heat extraction using three-dimensional thermo-hydro-chemical (THC) model. Geothermics 51, 46–62.
Pandey, S.N., Chaudhuri, A., Rajaram, H., Kelkar, S., 2015. Fracture transmissivity evolution due to silica dissolution/precipitation during geothermal heat extraction. Geothermics 57, 111–126.
Pandey, S.N., Chaudhuri, A., Kelkar, S., 2017. A coupled thermo-hydro-mechanical modeling of fracture aperture alteration and reservoir deformation during heat extraction from a geothermal reservoir. Geothermics 65, 17–31.
Peters, E., Blöcher, G., Salimzadeh, S., Egberts, P.J.P., Cacace, M., 2018. Modelling of multi-lateral well geometries for geothermal applications. Adv. Geosci. 45, 209–215.
Phillips, 1992. Flow and Reactions in Permeable Rocks. Cambridge University Press.
Puso, M.A., Laursen, T.A., 2004. A mortar segment-to-segment contact method for large deformation solid mechanics. Comput. Methods Appl. Mech. Eng. 193 (6–8), 601–629.
Rawal, C., Ghassemi, A., 2014. A reactive thermo-poroelastic analysis of water injection into an enhanced geothermal reservoir. Geothermics 50, 10–23.
Rimstidt, J.D., Barnes, H.L., 1980. The kinetics of silica-water reactions. Geochimica et Cosmochimica Acta 44, 1683–1699.
Salimzadeh, S., Paluszny, A., Zimmerman, R.W., 2016. Thermal effects during hydraulic fracturing in low-permeability brittle rocks. 50th US Rock Mechanics / Geomechanics Symposium 2016, vol. 1.
Salimzadeh, S., Nick, H.M., Zimmerman, R.W., 2018a. Thermoporoelastic effects during heat extraction from low-permeability reservoirs. Energy 142, 546–558.
Salimzadeh, S., Paluszny, A., Zimmerman, R.W., 2018b. Effect of cold CO2 injection on

fracture apertures and growth. Int. J. Greenh. Gas Control 74, 130–141.
Salimzadeh, S., Grandahl, M., Medetbekova, M., Nick, H.M., 2019. A novel radial jet drilling stimulation technique for enhancing heat recovery from fractured geothermal reservoirs. Renew. Energy 139, 395–409.
Stüben, K., 2001. A review of algebraic multigrid. J. Comput. Appl. Math. 128 (1–2), 281–309.
Szymczak, P., Ladd, A.J.C., 2006. A network model of channel competition in fracture dissolution. Geophys. Res. Lett. 33 (no. 5), 1–5.
Taron, J., Elsworth, D., Min, K.B., 2009. Numerical simulation of thermal-hydrologic-mechanical-chemical processes in deformable, fractured porous media. Int. J. Rock Mech. Min. Sci. (1997).
Usui, T., Salimzadeh, S., Paluszny, A., Zimmerman, R.W., 2017. Effect of poroelasticity on hydraulic fracture interactions. Poromechanics 2017 - Proceedings of the 6th Biot Conference on Poromechanics.
Vik, H., Salimzadeh, S., Nick, H.M., 2018. Heat recovery from multiple-fracture enhanced geothermal systems: the effect of thermoelastic fracture interactions. Renew. Energy 121, 606–622.
Walsh, S.D.C., Garapati, N., Leal, A.M.M., Saar, M.O., 2017. Calculating thermophysical fluid properties during geothermal energy production with NESS and Reaktoro. Geothermics 70, 146–154.
Wriggers, P., Zavarise, G., 1993. Application of augmented Lagrangian techniques for Non-linear constitutive laws in contact interfaces. Commun. IN Numer. Methods Eng. 9, 815–824.
Zimmerman, R.W., Bodvarsson, G.S., 1996. Hydraulic conductivity of rock fractures. Transp. Porous Media 23, 1–30.